ACS Catalysis

Research Article

Cite This: ACS Catal. 2019, 9, 4394−4401

pubs.acs.org/acscatalysis

Equatorial Active Site Compaction and Electrostatic Reorganization in Catechol-*O*-methyltransferase

Sylwia Czarnota,[†,‡] Linus O. Johannissen,[†] Nicola J. Baxter,[§] Felix Rummel,[†,‡] Alex L. Wilson,[†,‡] Matthew J. Cliff,[†] Colin W. Levy,[†] Nigel S. Scrutton,[†,‡] Jonathan P. Waltho,[†,‡,§] and Sam Hay*[,†,‡]

[†]Manchester Institute of Biotechnology, The University of Manchester, 131 Princess Street, Manchester, M1 7DN, United Kingdom

[‡]School of Chemistry, The University of Manchester, Oxford Road, Manchester, M13 9PL, United Kingdom

[§]Krebs Institute for Biomolecular Research, Department of Molecular Biology and Biotechnology, The University of Sheffield, Firth Court, Western Bank, Sheffield, S10 2TN, United Kingdom

Supporting Information

ABSTRACT: Catechol-*O*-methyltransferase (COMT) is a model S-adenosyl-L-methionine (SAM) dependent methyl transferase, which catalyzes the methylation of catecholamine neurotransmitters such as dopamine in the primary pathway of neurotransmitter deactivation in animals. Despite extensive study, there is no consensus view of the physical basis of catalysis in COMT. Further progress requires experimental data that directly probes active site geometry, protein dynamics and electrostatics, ideally in a range of positions along the reaction coordinate. Here we establish that sinefungin, a fungal-derived inhibitor of SAM-dependent enzymes that possess transition state-like charge on the transferring group, can be used as a transition state analog of COMT when combined with a catechol. X-ray crystal structures and NMR backbone assignments of the ternary complexes of the soluble form of human COMT containing dinitrocatechol, Mg^{2+} and SAM or sinefungin were determined. Comparison and further analysis with the aid of density functional theory calculations and molecular dynamics simulations provides evidence for active site "compaction", which is driven by electrostatic stabilization between the transferring methyl group and "equatorial" active site residues that are orthogonal to the donor−acceptor (pseudo reaction) coordinate. We propose that upon catecholamine binding and subsequent proton transfer to Lys 144, the enzyme becomes geometrically preorganized, with little further movement along the donor−acceptor coordinate required for methyl transfer. Catalysis is then largely facilitated through stabilization of the developing charge on the transferring methyl group via "equatorial" H-bonding and electrostatic interactions orthogonal to the donor−acceptor coordinate.

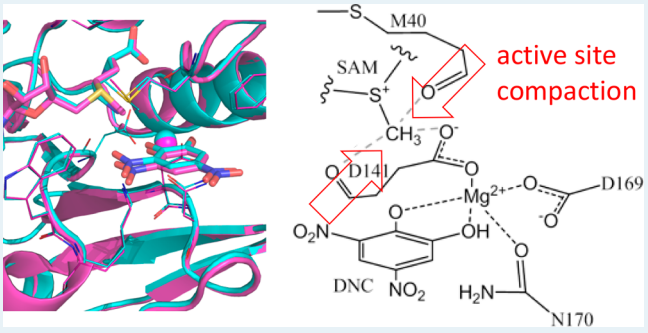

KEYWORDS: *enzyme, S-adenosyl-L-methionine, sinefungin, NMR, X-ray crystallography, molecular dynamics simulation, density functional theory*

INTRODUCTION

S-Adenosyl-L-methionine (SAM) dependent methyl transferases (MTases) are ubiquitous bisubstrate Mg^{2+}-dependent enzymes found in plants, animals, and microorganisms. Catechol-*O*-methyltransferase (COMT) is an archetypal MTase, which catalyzes the methylation of catecholamine neurotransmitters such as dopamine in the primary pathway of neurotransmitter deactivation in animals. Consequently, inhibition of COMT is a key strategy for the treatment of a range of neurological disorders including Parkinson's disease.[1−3] COMT also has potential as a biocatalyst for regiospecific alkylation reactions, for example, refs 4 and 5, and has long served as a model MTase enzyme. In this family of enzymes, methyl transfer is proposed to occur by a common S_N2 mechanism with nucleophilic attack on the SAM methyl group from the methyl accepting substrate (catechol hydroxyl in COMT). The Mg^{2+} ion is bound between the catechol oxygens, facilitating deprotonation of the catechol in order to render it a more potent nucleophile. The transferring methyl group proceeds with net inversion of configuration, adopting an sp^2-like geometry in the transition state (TS; Figure 1). For COMT, the catalytic enhancement has been estimated from experimental data to be on the order of 10^9 to 10^{16}.[6,7]

A major feature of the COMT reaction is that the reactant state comprises oppositely charged reactants, which combine to form neutral products; that is, a CH_3^+ group is formerly transferred. This might suggest that electrostatics (pre/reorganization) should play a major role in the reaction of COMT and related MTases, as has been argued by some, for example, refs 6 and 8−10. However, kinetic isotope effect

Received: January 14, 2019
Revised: March 26, 2019
Published: April 9, 2019

DOI: 10.1021/acscatal.9b00174
ACS Catal. 2019, 9, 4394−4401

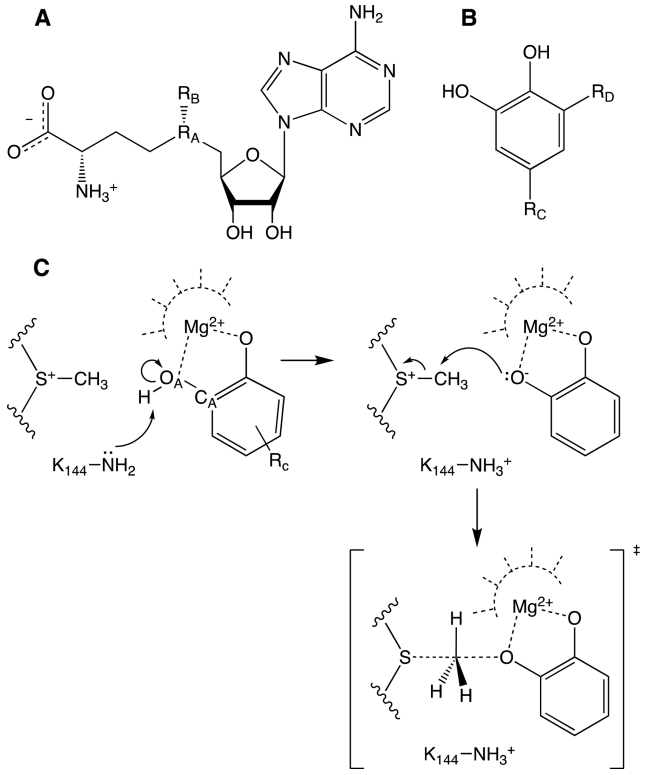

Figure 1. A, The structures of A, S-adenosyl-L-methionine (SAM, R_A=S^+, R_B=CH_3), and sinefungin (R_A=CH, R_B=NH_3^+), B, 3,5-dinitrocatechol (DNC, R_C=R_D=NO_2) and dopamine (R_C=$CH_2CH_2NH_2$, R_D=H). C, The proposed mechanism of SAM demethylation catalyzed by COMT. For many catecholamine substrates both oxygen atoms can act as the methyl acceptor, with the stereochemistry determined by the catecholamine binding position; the oxygen closer to the transferring methyl is the acceptor.

(KIE) measurements from the Schowen group in the late 1970s showed an unusually large and inverse CH_3/C^2H_3 KIE of ~0.8 for the COMT reaction[11] with much smaller KIEs observed on uncatalyzed model methyl transfer reactions.[7] These data, alongside more recent KIE measurements from the Klinman group showing a correlation between k_{cat}/K_m and CH_3/C^3H_3 KIEs on the COMT reaction,[12] have been used as evidence for the role of active site compression or "compaction" during the reaction;[7,13] essentially the squeezing together of the reacting methyl donor and acceptor moieties, which promotes the reaction. This description is couched within the framework of the "promoting vibration" hypothesis, which has been used to interpret isotope effects on H-transfer reactions.[14−16] The unusual deuterium KIE on the COMT reaction has also received much attention from the computational community, with a number of proposals put forward to describe catalysis by COMT. Ground state near attack conformers (NACs) have been proposed by Bruice,[17,18] whereas Warshel has recently argued against compaction and NACs in favor of electrostatic preorganization.[8] Williams and colleagues also saw no evidence for compaction[6,19,20] and highlighted the role of equatorial H-bonding to the transferring methyl group.[21] Finally, Klinman and Martinez recently observed a trend in donor−acceptor distance in the ground state that they correlate with catalytic efficiency, in favor of the compaction hypothesis.[12,13]

It would appear that there is no consensus view of the physical basis of catalysis in COMT. A major issue is that computational studies are based on relatively few experimental data: X-ray crystal structures of nonreactive inhibitor (e.g., DNC; Figure 1) and drug complexes, KIE measurements of COMT and reference reactions and steady state inhibition assays, for example. ref 22. We suggest that progress toward a consensus description of catalysis by COMT, and by extension the MTase enzyme family, requires new experimental data that directly probes active site geometry, protein dynamics and electrostatics, ideally in a range of positions along the reaction coordinate; at a minimum the reactant state and TS.

Sinefungin (adenosyl-L-ornithine), a fungal-derived inhibitor of SAM-dependent MTases,[23] is a nonreactive SAM-analogue with an amine group in place of the transferring methyl group and a CH in place of the sulfur (Figure 1A). As the amine group is likely to be protonated,[24] it should have a more TS-like charge distribution than SAM. Sinefungin derivatives are also known to be good TS analogues of the SAM-dependent lysine methyl transferase,[25] so ternary complexes of COMT containing sinefungin, Mg^{2+} and an appropriate catechol should provide a means to probe COMT in a more TS-like conformation. X-ray crystal structures of sinefungin complexes of MTases have been solved including rat COMT (PDB 4P7K; binary complex without catechol) and "humanized" rat COMT (PDB 4PYL; ternary complex containing the drug tolcapone).[26] Here we have determined the X-ray crystal structures and NMR backbone assignments of the ternary complexes of the soluble form of human COMT (S-COMT) containing DNC, Mg^{2+} and both SAM or sinefungin. These complexes are compared and further analyzed with the aid of density functional theory (DFT) calculations and molecular dynamics (MD) simulations. We find evidence for active site compaction and propose that this is driven by H-bonding between the transferring methyl group and "equatorial" active site residues, rather than by "pushing" along the donor−acceptor axis.

RESULTS AND DISCUSSION

As sinefungin contains partial TS character, the sinefungin complex will represent a reactant pose that is positioned along the reaction coordinate between the ground state and TS (or further) and any conformational change/reorganization that occurs between SAM and sinefungin ternary complexes is likely to be relevant to catalysis. It should therefore be possible to experimentally probe COMT reorganization during the reaction by comparing equivalent ternary complexes containing sinefungin and SAM.

We screened a range of catecholamine substrates and inhibitors and were able to obtain crystals of S-COMT complexes containing Mg^{2+}, DNC and both sinefungin or SAM. These diffracted to 1.3−1.5 Å and the structures were readily solved by molecular replacement (Figure 2 and Supporting Information (SI) Table S1). The sinefungin complex crystallized as a dimer while the SAM complex crystallized as a monomer (see also SI Figure S1), but the structures are largely superimposable and are similar to existing structures of S-COMT containing SAM and DNC (e.g., PDB 3BWM[27] and SI Table S2). The two monomers in the sinefungin complex are not identical, but are very similar, with key active site distances differing by <0.03 Å (Table 1, SI Figure S2). S-COMT is known to dimerize[28] and each monomer is structurally nearly identical to the SAM-bound structure (Figure 2), so we propose these structures are likely to represent active conformations of the enzyme.

DOI: 10.1021/acscatal.9b00174
ACS Catal. 2019, 9, 4394−4401

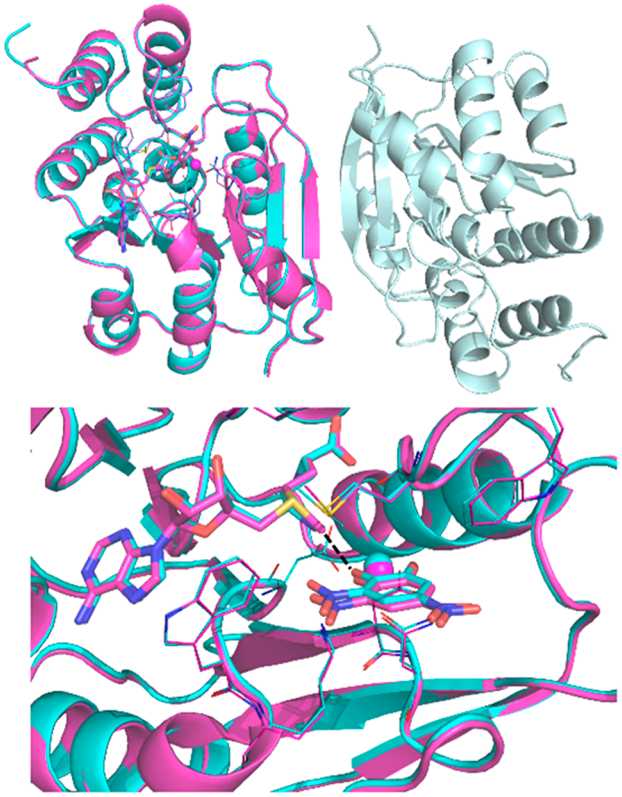

Figure 2. X-ray crystal structures of S-COMT ternary complexes containing DNC, Mg^{2+} and either SAM (magenta) or sinefungin (cyan, light green). Structures are aligned over all atoms and the bottom panel shows an overlay of the active site region with selected residues displayed as wireframes, SAM, sinefungin, and DNC shown as sticks and the Mg^{2+} ion indicated as a sphere. The O−CH_3 distance is indicated with a dashed black line.

Table 1. Key Reactant Distances (R) and Angles (A)[a] Observed in The X-ray Crystal Structures in Figure 2 and SI Figure S2

	ternary complex	
	SAM	sinefungin[b]
R(D-A), Å	4.57	4.20, 4.22
R(X-A), Å	2.81	2.71, 2.74
R(D-X), Å	1.78	1.51, 1.50
A(D-X-A), °	169	170, 169
A(X-A-C_A), °	114	115, 117

[a]D, donor; A, acceptor; X, transferring group (CH_3 or NH_3); C, DNC C_A (Figure 1). [b]Measured in chain A and chain B, respectively.

Within the respective ternary complexes, SAM and sinefungin adopt very similar conformations and the only large difference is the position of the DNC, which is closer to the sinefungin than to SAM (Figure 2; Table 1). This may arise, in part, as the C−NH_3 bond of sinefungin is significantly shorter than the S−CH_3 bond of SAM (Table 1).

The distances observed between the acceptor oxygen atom and transferring CH_3 or NH_3 groups (denoted R(X-A) here) are both shorter than the expected sum of van der Waals radii. This behavior is observed in the X-ray crystal structures of other COMT ternary complexes (SI Table S2) and has been suggested to arise due to the presence of the anionic (deprotonated) form of the catechol.[13] Further inspection of other X-ray crystal structures of ternary complexes of COMT show considerable variability in the R(X-A) distances and those between the donor sulfur and acceptor oxygen (denoted R(D-A)). However, when only considering relatively high-resolution structures (<2.0 Å) containing DNC, the R(X-A) values are in good agreement at ∼2.7−2.8 Å and those structures containing SAM have R(D-A) values of ∼4.5−4.6 Å. The sinefungin R(D-A) values determined in the current study and previously in the sinefungin-tolcapone ternary complex (PDB 4PYL) are notably shorter, likely due at least in part to the shorter C−NH_3 bond of sinefungin. In the present study, R(X-A) and R(D-A) are shorter by ∼0.1 and 0.35 Å, respectively, in the sinefungin complex vs the SAM complex. While the shorter R(X-A) may not be statistically significant, collectively this movement is consistent with the movement of the catecholamine toward the SAM, which is expected to occur upon moving from the reactant state to the TS in order to facilitate O−CH_3 bond formation.

As the reaction occurs via an S_N2 mechanism, the angle between the donor sulfur, transferring methyl carbon and acceptor oxygen should ideally be ∼180° in the transition state. This angle is very similar for both sinefungin and SAM complexes, and as this angle is almost 170°, there is minimal reorganization required to achieve an ideal S_N2 geometry. Similarly, the angle formed between the transferring group, catecholamine acceptor oxygen, and catecholamine C_A (Figure 1) should ideally be ∼110−120°. It is ∼115° and is slightly larger in the sinefungin complex. Together, these data show a structurally preorganized active site with only minimal rearrangement of substrate (catecholamine) required to reach the anticipated TS geometry.

As mentioned above, the crystal structures for the SAM and sinefungin complexes are nearly identical. However, X-ray crystallography may not have sufficient resolution to resolve subtle protein reorganization, so we next turned to NMR to further probe these complexes. We have previously reported the backbone ^1H, ^{15}N and ^{13}C NMR chemical shift assignments of the S-COMT:SAM:DNC:Mg^{2+} ternary complex.[28] We used the same approach here to determine the equivalent assignments in the S-COMT:sinefungin:DNC:Mg^{2+} ternary complex. The S-COMT construct contains 233 residues, and excluding the 10 proline residues and 8 residues of the N-terminal His-tag there are 215 observable residues. 204 of these residues were assigned in the $^1H-^{15}N$ TROSY spectrum of the sinefungin complex (SI Figure S3). Protein secondary structure prediction using the backbone ^1H_N, ^{15}N, $^{13}C_\alpha$, $^{13}C_\beta$, and $^{13}C'$ chemical shifts and the TALOS+ and TALOS-N algorithms, which are empirically defined models based on a correlation of experimental NMR chemical shift and X-ray crystal structure data,[29,30] is consistent with the solution conformation being very similar to both our, and previous X-ray crystal structures (SI Figure S4).[27]

Comparison of the differences in NMR chemical shifts between assigned residues in the SAM and sinefungin ternary complexes allows changes in the local environment of the protein backbone to be determined. Figure 3 shows the residue-by-residue difference in backbone amide nitrogen (N_H) chemical shift between the two complexes. These can be mapped onto the X-ray crystal structure and most differences are seen to be in the active site. A similar pattern is observed when analyzing the equivalent differences in H_N, Cα, Cβ, C′, and N−H chemical shifts (SI Figure S5).

The general trend in N_H chemical shift changes is an increase in chemical shift from the SAM to the sinefungin

DOI: 10.1021/acscatal.9b00174
ACS Catal. 2019, 9, 4394−4401

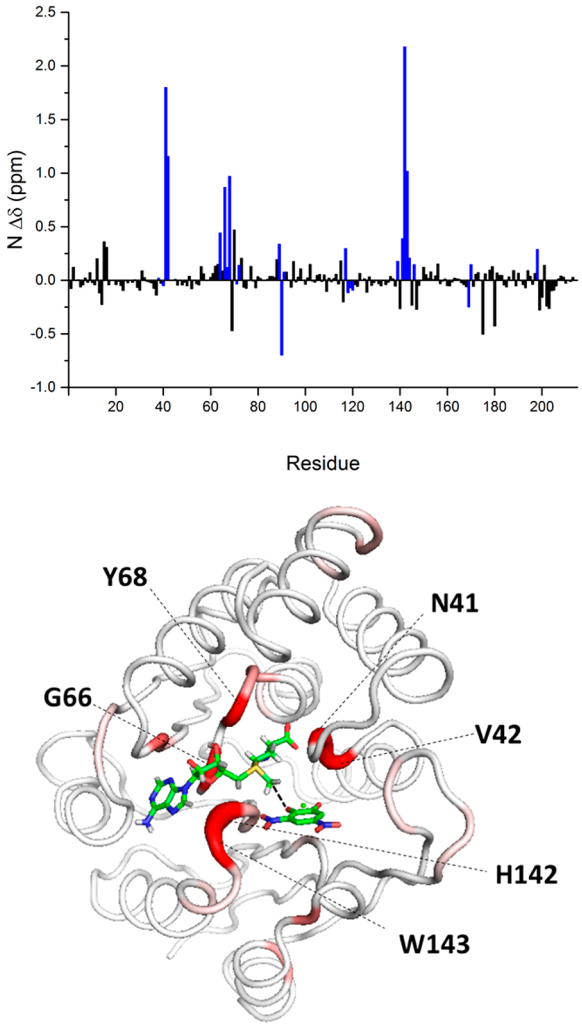

Figure 3. Differences in NMR chemical shift of the backbone amide atoms (N_H) between the S-COMT:SAM:DNC:Mg^{2+} and S-COMT:sinefungin: DNC:Mg^{2+} ternary complexes shown as a function of residue number (above) and as a putty diagram rendered on the X-ray crystal structure of the SAM complex (bottom). Active site residues within 4 Å of the SAM or DNC are shown as blue bars in (A) and the putty diagram is colored from low (white) to high (red) difference in chemical shift. The O−CH_3 distance between SAM and DNC is indicated with a dashed black line. The equivalent differences in H_N, Cα, Cβ, C′, and N−H chemical shifts are shown in SI Figure S5.

ternary complex (Figure 3). This trend is also reflected in the H_N chemical shifts (SI Figure S5) and is consistent with an increase in proximity of the hydrogen bond acceptor for the amide.[31] However, the residues with the largest chemical shift differences are not all involved in structural hydrogen bonds and the chemical shift differences will also include contributions from torsional angle changes and hydrogen bond donor to the peptide carbonyl. The largest N_H chemical shift differences observed are in the following residues: V42, which is hydrogen-bonded to the carboxyl oxygens of SAM/sinefungin and the neighboring N41 and M40 residues, which are also in close proximity to the transferring methyl group; Y68, which is positioned behind the SAM sulfur (relative to the transferring group) and the neighboring G66 and A67 residues; H142 and W143, which are both in van der Waals contacts with the adenine moiety of SAM; D141, which is hydrogen-bonded to the amino group of the methionine moiety of SAM and also coordinates the Mg^{2+} ion. These chemical shift differences can all be rationalized in terms of subtle conformational differences in the active sites of the two ternary complexes, which may not be observable in the comparison of ∼1.4 Å resolution X-ray crystal structures (as in Figure 2). To extend this analysis, we next turned to computational chemistry.

First, active site "cluster" models were used to analyze the change in charge distribution of SAM between the reactant and TS states. These models were based on the X-ray crystal structure of the SAM ternary complex and comprised the active site region containing Mg^{2+}, SAM and catechol in place of the nonreactive DNC. Two sets of models were used to ensure that qualitatively the charge distribution is not model specific; one was comprised of ∼580 atoms, many of which had positional constraints (SI Figure S6) while the other was comprised of ∼220 atoms, with minimal positional constraints (SI Figure S7). The DFT models are described further in the SI and key parameters are given in Table 2 and SI Table S4. An approximate TS was determined for the reaction by performing a (partially) relaxed scan and the potential energy barrier was found to be 66 kJ mol^{-1} and 59 kJ mol^{-1} for the large and smaller models, respectively. The free energy barrier for the smaller model was also estimated to be 62 kJ mol^{-1} using normal-mode analysis. These values are comparable to the experimental free energy of activation, which is ∼75 kJ mol^{-1},[32] and to previous QM/MM-computed free energy barriers of, for example, 87 kJ mol^{-1},[6] 69 kJ mol^{-1},[33] and 67 kJ mol^{-1}.[34]

Table 2. Selected Distances (R, Å), Angles (A, °) and Charges in the ∼220 Atom DFT Cluster Models

	SAM:catechol.:Mg^{2+}[a]		DNC:Mg^{2+},[b]	
	reactant	TS	SAM	sinefungin
R(D-A)[c]	4.61	4.55	4.63	4.30
R(X-A)[c]	2.79	2.08	2.82	2.80
R(D-X)[c]	1.83	2.48	1.82	1.51
A(D-X-A)	172	177	172	172
A(X-A-C_A)	99	110	101	114
q(D)[c]	0.81	0.39	0.81	0.20
q(A)[c]	−0.91	−0.81	−0.79	−0.80
q(XH_3)[c]	0.08	0.36	0.06	0.63

[a]Reactant state and approximate TS in a model containing SAM, Mg^{2+} and catechol in place of DNC. The approximate TS geometry was obtained from a relaxed scan of R(X-A). [b]Reactant state models containing DNC, Mg^{2+} and SAM or sinefungin. [c]Distances (R) and angles (A) are equivalent to those given in Table 1; q(D), q(A) and q(XH_3) are the natural charge on the donor, acceptor and summed over the transferring group, respectively.

As expected, in both cluster models R(D-A) and R(X-A) are shorter in the TS than the reactant state, while R(D-X) is longer. The reduction in R(D-A) is smaller in the smaller cluster model (∼0.1 cf. ∼ 0.2 Å), which may be due to the absence of the Y68 in this model as Y68 has previously been suggested to play a role in maintaining a short D−A distance.[13] In both models the charge on the transferring methyl group significantly increases upon moving from the reactant to TS, with a concomitant decrease in charge on the SAM sulfur. There is little change in the acceptor oxygen, which is

DOI: 10.1021/acscatal.9b00174
ACS Catal. 2019, 9, 4394−4401

consistent with the dissociative TS proposed for similar MTases.[e.g.24,35]

Next, the two models were modified to describe ternary complexes containing Mg^{2+}, DNC and SAM or sinefungin (Table 2, SI Table S4 and Figures S6 and S7). As DNC is nonreactive, only the reactant state was considered. In both the smaller and larger models, R(D-A) is ~0.3 Å shorter in the sinefungin complex than the SAM complex, suggesting that the sinefungin complex adopts a more TS-like geometry. Additionally, the larger cluster models support the protonation state of the sinefungin NH_3^+ group, as replacing this with NH_2 causes a significant shift in the position of DNC that is inconsistent with the crystal structure (SI Figure S6d).

Crucially, the differences in charge distribution between the reactant state and TS of the SAM-catechol model is qualitatively similar to the difference in charge distribution of the SAM and sinefungin DNC models; that is, the positive charge that develops on the transferring SAM methyl group is similar to that observed on the sinefungin NH_3 group (Table 2 and SI Table S4), and there is little change to the charge on the acceptor oxygen. On the other hand, the partial charge on the sinefungin NH_3 is larger than that on the SAM CH_3 in the TS, suggesting that any resulting protein electrostatic rearrangement upon sinefungin binding may be somewhat greater than for the actual reaction. Nevertheless, these calculations suggest that the COMT:sinefungin:DNC:Mg^{2+} ternary complex has considerable TS character, both in terms of overall geometry and electrostatics.

MD simulations were next performed on the S-COMT:SAM:DNC:Mg^{2+} and S-COMT:sinefungin:DNC:Mg^{2+} ternary complexes, using the X-ray crystal structures as input structures. DFT cluster models were used to parametrize the substrates and octahedral Mg^{2+} (see SI for details) and the sinefungin complex was treated as a monomer to aid in the comparison with the SAM complex. Simulations were typically run for 50−100 ns using the Amber 14 force field (note that we are only looking at small changes in the active site). To check the consistency between NMR, crystallography, and MD data, phi (Φ) and psi (Ψ) torsion angles values obtained using the three approaches were compared (SI Figures S8 and S9) and show generally good agreement between all methods.

Analysis of MD data to determine differences between the two complexes focused on the distance between the donor atom, D (S1 in SAM) and the Cα of the first-shell active site residues that exhibit, or are neighboring residues that exhibit large differences in NMR chemical shifts (Figure 3). This reveals a compression or compaction between residues 40−42 and 141−142, which are situated in loops on either side of the catecholamine binding pocket, in the sinefungin complex relative to the SAM complex (Figure 4 and SI Figure S10). Such compaction is consistent with these regions showing large changes in NMR chemical shift. The donor−Y68Cα distance is longer in the sinefungin complex than in the SAM complex, which is also consistent with the NMR shift differences observed in Figure 3 and SI Figure S5. This is qualitatively consistent with the crystal structures, where a (albeit negligible) 0.03−0.04 Å increase in the donor−Y68Cα distance is observed between the SAM and sinefungin structures. It has been proposed that Y68 is crucial for the positioning of SAM and maintaining an optimal donor−acceptor distance.[13] Our results are consistent with this as the difference observed here arises in part due to the extra hydrogen atom in sinefungin (as S1 is replaced by CH; see SI)

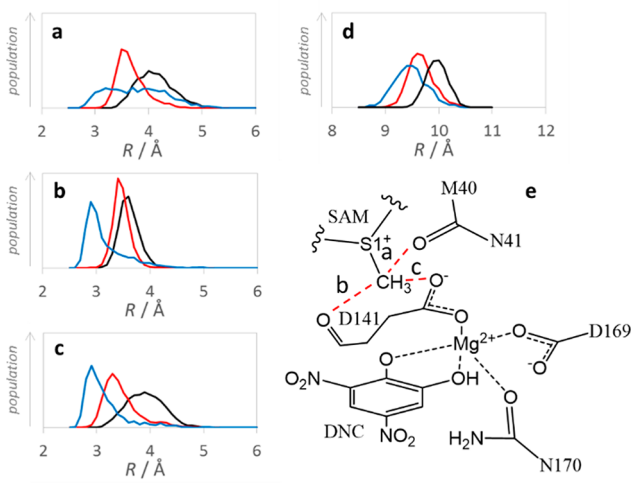

Figure 4. Active site compaction. S1−M40O (a), S1−D141O (b), S1−D141OD2 (c), M40Cα-D141Cα (d) distance distributions during MD simulations of tertiary complexes containing SAM (black), SAM* (red) and sinefungin (blue). An active site illustration showing distances a-c is shown in (e). Additional distances are plotted in SI Figure S10.

as well as the stronger compaction causing M40 to push against Y68 (SI Figure S11).

To determine whether the observed active site compaction is purely driven by electrostatics, MD simulations were also performed with an artificial SAM molecule containing sinefungin-like charges on the donor and transferring methyl groups. This molecule is denoted SAM* and SI Table S5 contains more details of the charges used. The degree of compaction was found to be greater for sinefungin than SAM*, likely reflecting differences in the chemical structure (NH_3 can form stronger H-bonds than CH_3) and geometry between SAM and sinefungin, but confirming that electrostatics clearly also plays a key role in this compaction. The increased positive charge on the sinefungin NH_3^+ (and SAM* methyl group) pulls nearby oxygen atoms toward it; these atoms include the backbone oxygen of M40, the backbone oxygen of D141 and the carboxyl group of D141 (Figure 4). Notably, there is a compaction of the loops on either side of the DNC, with a 0.5 Å decrease in the average M40Cα−D141Cα distance (Figure 4d). Again, this is qualitatively consistent with the crystal structure, where a 0.2 Å decrease is observed. This active site compaction is also consistent with the role of equatorial CH−O hydrogen bonds proposed by Wilson and Williams.[21]

To assess whether our proposed active site compaction is consistent with experimental data, we also ran MD simulations with selected backbone dihedrals restrained to values derived from our NMR data. Thus, restraints were applied to the backbone torsion angles of those residues with the largest differences observed between the SAM and sinefungin Φ and Ψ values derived using the TALOS-N algorithm. For all three complexes (SAM, SAM* and sinefungin), constraining selected Φ and Ψ torsion angles to the values from the sinefungin NMR data leads to active site compaction relative to simulations constrained to the SAM NMR values (SI Figure S12). Again, this confirms that the effects seen in the MD simulations are consistent with the NMR data and shows that compaction is driven, at least in part, by the protein backbone (cf. side chains).

DOI: 10.1021/acscatal.9b00174
ACS Catal. 2019, 9, 4394−4401

Finally, the effect of active site compaction on the electrostatic stabilization of sinefungin, and by inference the TS, was analyzed using energy decomposition; the energy of the system during each MD simulation was recalculated with and without charges on selected amino acids, and with either SAM or sinefungin charges applied to the SAM, SAM* or sinefungin molecule. This gives the relative stabilization energy, ΔE, of sinefungin relative to SAM by the amino acid in question. This analysis reveals that D141 dominates the electrostatic stabilization of sinefungin and SAM* (Figure 5 and SI Figure S13). D141 and M40 both preferentially stabilize sinefungin over SAM during the SAM simulation ($\Delta E < 0$), then as the SAM transferring methyl group acquires positive charge and the oxygen atoms of these two residues move closer in the SAM* and sinefungin simulations, this stabilization effect increases. On the other hand, K144 (the active site amino acid that initially deprotonates the substrate; Figure 1C) destabilizes sinefungin ($\Delta E > 0$), as expected for a positively charged residue. However, the change in ΔE for both K144 and M40 between the SAM, SAM* and sinefungin simulations is much smaller than that for D141, likely due to the net negative charge of D141 and its closer proximity to the developing positive charge on the transferring group.

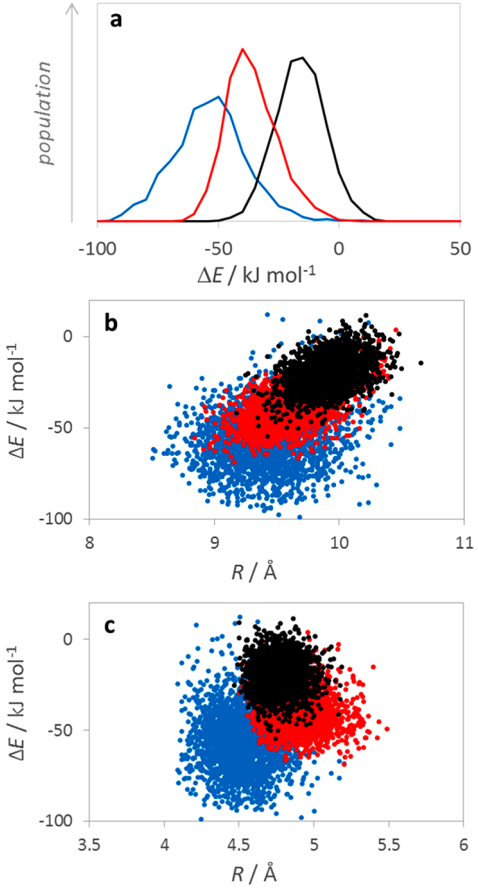

Figure 5. (a) Electrostatic stabilization of sinefungin and SAM* relative to SAM during SAM (black line), SAM* (red line) and sinefungin (blue line) MD simulations. Correlations between active site compaction. The M40Cα–D141Cα distance (b) and donor–acceptor distance (c) vs. D141 stabilization energy for the SAM (black), SAM* (red) and sinefungin (blue) simulations.

As ΔE is calculated for each MD snapshot, it is possible to observe how this fluctuates throughout the MD simulation. A significant correlation between the M40Cα–D141Cα distance and ΔE for D141 was observed, with larger stabilization observed when this distance is shorter and thus the active site is more compact along the "equatorial" plane orthogonal to the donor–acceptor axis.[21] This can be rationalized in terms of the expected distance dependence of the Coulombic interaction between D141 and the transferring group (which sits between M40 and D141) and shows a clear link between electrostatic stabilization and active site geometry (Figure 5b). Motion along the M40Cα–D141Cα and donor–acceptor coordinates are not correlated (SI Figure S14) and there is little correlation between ΔE and the donor–acceptor distance (Figure 5c). Our DFT calculations show small-negligible charge transfer from the acceptor oxygen to methyl group (Table 2, SI Table S4), which is consistent with previous proposals that MTases possess a loose or dissociative TS (for example, refs 24 and 35). We cannot rule out a role for donor–acceptor sampling in methyl transfer in COMT, particularly during the proton transfer from catechol to Lys 144, which apparently leads to the formation of a highly preorganized active site with short R(D-A). However, our NMR data and MD simulations do reveal that increased electrostatic stabilization at the methyl transfer TS is coupled to protein motion orthogonal to the donor–acceptor coordinate that allows the formation and/or strengthening of "equatorial" H-bonding and/or electrostatic interactions. This is likely to be consistent with the proposal that the unusual deuterium[11] and tritium[12] KIEs observed on the reaction arise, at least in part, through perturbations to the equatorial H-bonding.[21]

In summary, ternary complexes of COMT containing sinefungin, Mg^{2+} and a suitable catechol such as DNC possess some TS-like character; that is, they can be considered to be TS analogs. By comparison with the equivalent reactant state complex containing SAM, we can experimentally probe the protein reorganization relevant to catalysis. With the aid of DFT calculations and MD simulations, we have shown that active site compaction along the "equatorial" plane orthogonal to the donor–acceptor axis plays a key role in stabilizing the positive charge that develops on the transferring methyl group. As these interactions are largely independent of the catechol-amine methyl acceptor, such "equatorial" H-bonding and electrostatic interactions may be a general feature of catalysis by the SAM-dependent MTase family of enzymes.

EXPERIMENTAL DETAILS

Full computational and experimental details are given in the Supporting Information. X-ray crystal structure models of the S-COMT:SAM:DNC:Mg^{2+} and S-COMT:sinefungin:DNC:Mg^{2+} complexes have been deposited in the protein data bank with the accession codes 6I3C and 6I3D, respectively. The backbone ^{1}H, ^{13}C and ^{15}N chemical shift assignments for S-COMT:SAM:DNC:Mg^{2+} and S-COMT:sinefungin:DNC:Mg^{2+} have been deposited in the BioMagResBank under the BMRB accession codes 26848 and 26851, respectively.

ASSOCIATED CONTENT

Supporting Information

The Supporting Information is available free of charge on the ACS Publications website at DOI: 10.1021/acscatal.9b00174.

DOI: 10.1021/acscatal.9b00174
ACS Catal. 2019, 9, 4394–4401

Full computational and experimental details as well as additional supporting data (PDF)

AUTHOR INFORMATION

Corresponding Author

*E-mail: sam.hay@manchester.ac.uk.

ORCID

Nigel S. Scrutton: 0000-0002-4182-3500
Jonathan P. Waltho: 0000-0002-7402-5492
Sam Hay: 0000-0003-3274-0938

Author Contributions

The manuscript was written through contributions of all authors.

Notes

The authors declare no competing financial interest.

ACKNOWLEDGMENTS

This research was supported by a European Commission Marie Curie Fellowship (S.C. Grant number: PITN-GA-2013-ITN 606831), and in part by the UK Biotechnology and Biological Sciences Research Council (BBSRC; reference: BB/H021523/1). We acknowledge Diamond Light Source for time on beamlines i04 & i04-1 under proposal MX12788-32 and MX12788-41. We also acknowledge the assistance given by IT Services and the use of the Computational Shared Facility at The University of Manchester.

REFERENCES

(1) Fava, M.; Rosenbaum, J. F.; Kolsky, A. R.; Alpert, J. E.; Nierenberg, A. A.; Spillmann, M.; Moore, C.; Renshaw, P.; Bottiglieri, T.; Moroz, G.; Magni, G. Open Study of the Catechol-O-Methyltransferase Inhibitor Tolcapone in Major Depressive Disorder. *J. Clin. Psychopharmacol.* **1999**, *19*, 329−35.

(2) Kiss, L. E.; Soares-da-Silva, P. Medicinal Chemistry of Catechol O-Methyltransferase (COMT) Inhibitors and Their Therapeutic Utility. *J. Med. Chem.* **2014**, *57*, 8692−717.

(3) Harrison, S. T.; Poslusney, M. S.; Mulhearn, J. J.; Zhao, Z.; Kett, N. R.; Schubert, J. W.; Melamed, J. Y.; Allison, T. J.; Patel, S. B.; Sanders, J. M.; Sharma, S.; Smith, R. F.; Hall, D. L.; Robinson, R. G.; Sachs, N. A.; Hutson, P. H.; Wolkenberg, S. E.; Barrow, J. C. Synthesis and Evaluation of Heterocyclic Catechol Mimics as Inhibitors of Catechol-O-Methyltransferase (COMT). *ACS Med. Chem. Lett.* **2015**, *6*, 318−23.

(4) Li, K.; Frost, J. W. Synthesis of Vanillin from Glucose. *J. Am. Chem. Soc.* **1998**, *120*, 10545−10546.

(5) Law, B. J.; Bennett, M. R.; Thompson, M. L.; Levy, C.; Shepherd, S. A.; Leys, D.; Micklefield, J. Effects of Active-Site Modification and Quaternary Structure on the Regioselectivity of Catechol-O-Methyltransferase. *Angew. Chem., Int. Ed.* **2016**, *55*, 2683−7.

(6) Roca, M.; Marti, S.; Andres, J.; Moliner, V.; Tunon, I.; Bertran, J.; Williams, I. H. Theoretical Modeling of Enzyme Catalytic Power: Analysis of "Cratic" and Electrostatic Factors in Catechol O-Methyltransferase. *J. Am. Chem. Soc.* **2003**, *125*, 7726−37.

(7) Mihel, I.; Knipe, J. O.; Coward, J. K.; Schowen, R. L. Alpha.-Deuterium Isotope Effects and Transition-State Structure in an Intramolecular Model System for Methyl-Transfer Enzymes. *J. Am. Chem. Soc.* **1979**, *101*, 4349−4351.

(8) Lameira, J.; Bora, R. P.; Chu, Z. T.; Warshel, A. Methyltransferases Do Not Work by Compression, Cratic, or Desolvation Effects, but by Electrostatic Preorganization. *Proteins: Struct., Funct., Genet.* **2015**, *83*, 318−30.

(9) Roca, M.; Andrés, J.; Moliner, V.; Tuñón, I.; Bertrán, J. On the Nature of the Transition State in Catechol O-Methyltransferase. A Complementary Study Based on Molecular Dynamics and Potential Energy Surface Explorations. *J. Am. Chem. Soc.* **2005**, *127*, 10648−10655.

(10) Świderek, K.; Tuñón, I.; Williams, I. H.; Moliner, V. Insights on the Origin of Catalysis on Glycine N-Methyltransferase from Computational Modeling. *J. Am. Chem. Soc.* **2018**, *140*, 4327−4334.

(11) Hegazi, M. F.; Borchardt, R. T.; Schowen, R. L. Alpha.-Deuterium and Carbon-13 Isotope Effects for Methyl Transfer Catalyzed by Catechol O-Methyltransferase. SN2-Like Transition State. *J. Am. Chem. Soc.* **1979**, *101*, 4359−4365.

(12) Zhang, J.; Klinman, J. P. Enzymatic Methyl Transfer: Role of an Active Site Residue in Generating Active Site Compaction That Correlates with Catalytic Efficiency. *J. Am. Chem. Soc.* **2011**, *133*, 17134−7.

(13) Zhang, J.; Kulik, H. J.; Martinez, T. J.; Klinman, J. P. Mediation of Donor-Acceptor Distance in an Enzymatic Methyl Transfer Reaction. *Proc. Natl. Acad. Sci. U. S. A.* **2015**, *112*, 7954−9.

(14) Hay, S.; Scrutton, N. S. Good Vibrations in Enzyme-Catalysed Reactions. *Nat. Chem.* **2012**, *4*, 161−8.

(15) Schramm, V. L.; Schwartz, S. D. Promoting Vibrations and the Function of Enzymes. Emerging Theoretical and Experimental Convergence. *Biochemistry* **2018**, *57*, 3299−3308.

(16) Klinman, J. P.; Offenbacher, A. R.; Hu, S. Origins of Enzyme Catalysis: Experimental Findings for C-H Activation, New Models, and Their Relevance to Prevailing Theoretical Constructs. *J. Am. Chem. Soc.* **2017**, *139*, 18409−18427.

(17) Lau, E. Y.; Bruice, T. C. Importance of Correlated Motions in Forming Highly Reactive near Attack Conformations in Catechol O-Methyltransferase. *J. Am. Chem. Soc.* **1998**, *120*, 12387−12394.

(18) Lau, E. Y.; Bruice, T. C. Comparison of the Dynamics for Ground-State and Transition-State Structures in the Active Site of Catechol O-Methyltransferase. *J. Am. Chem. Soc.* **2000**, *122*, 7165−7171.

(19) Kanaan, N.; Ruiz Pernia, J. J.; Williams, I. H. Qm/Mm Simulations for Methyl Transfer in Solution and Catalysed by Comt: Ensemble-Averaging of Kinetic Isotope Effects. *Chem. Commun.* **2008**, 6114−6.

(20) Ruggiero, G. D.; Williams, I. H.; Roca, M.; Moliner, V.; Tuñón, I. Qm/Mm Determination of Kinetic Isotope Effects for Comt-Catalyzed Methyl Transfer Does Not Support Compression Hypothesis. *J. Am. Chem. Soc.* **2004**, *126*, 8634−8635.

(21) Wilson, P. B.; Williams, I. H. Influence of Equatorial CH-O Interactions on Secondary Kinetic Isotope Effects for Methyl Transfer. *Angew. Chem., Int. Ed.* **2016**, *55*, 3192−5.

(22) Tunnicliff, G.; Ngo, T. T. Kinetics of Rat Brain Soluble Catechol-O-Methyltransferase and Its Inhibition by Substrate Analogues. *Int. J. Biochem.* **1983**, *15*, 733−8.

(23) Borchardt, R. T.; Eiden, L. E.; Wu, B.; Rutledge, C. O. Sinefungin, a Potent Inhibitor of S-Adenosylmethionine: Protein O-Methyltransferase. *Biochem. Biophys. Res. Commun.* **1979**, *89*, 919−924.

(24) Stratton, C. F.; Poulin, M. B.; Du, Q.; Schramm, V. L. Kinetic Isotope Effects and Transition State Structure for Human Phenylethanolamine N-Methyltransferase. *ACS Chem. Biol.* **2017**, *12*, 342−346.

(25) Zheng, W.; Ibáñez, G.; Wu, H.; Blum, G.; Zeng, H.; Dong, A.; Li, F.; Hajian, T.; Allali-Hassani, A.; Amaya, M. F.; Siarheyeva, A.; Yu, W.; Brown, P. J.; Schapira, M.; Vedadi, M.; Min, J.; Luo, M. Sinefungin Derivatives as Inhibitors and Structure Probes of Protein Lysine Methyltransferase SETD2. *J. Am. Chem. Soc.* **2012**, *134*, 18004−18014.

(26) Ehler, A.; Benz, J.; Schlatter, D.; Rudolph, M. G. Mapping the Conformational Space Accessible to Catechol-O-Methyltransferase. *Acta Crystallogr., Sect. D: Biol. Crystallogr.* **2014**, *70*, 2163−74.

(27) Rutherford, K.; Le Trong, I.; Stenkamp, R. E.; Parson, W. W. Crystal Structures of Human 108v and 108m Catechol O-Methyltransferase. *J. Mol. Biol.* **2008**, *380*, 120−30.

(28) Czarnota, S.; Baxter, N. J.; Cliff, M. J.; Waltho, J. P.; Scrutton, N. S.; Hay, S. (1)H, (15)N, (13)C Backbone Resonance Assignments of Human Soluble Catechol O-Methyltransferase in Complex with S-

DOI: 10.1021/acscatal.9b00174
ACS Catal. 2019, 9, 4394−4401

Adenosyl-L-Methionine and 3,5-Dinitrocatechol. *Biomol. NMR Assignments* **2017**, *11*, 57−61.
(29) Shen, Y.; Delaglio, F.; Cornilescu, G.; Bax, A. TALOS+: A Hybrid Method for Predicting Protein Backbone Torsion Angles from NMR Chemical Shifts. *J. Biomol. NMR* **2009**, *44*, 213−23.
(30) Shen, Y.; Bax, A. Protein Backbone and Sidechain Torsion Angles Predicted from NMR Chemical Shifts Using Artificial Neural Networks. *J. Biomol. NMR* **2013**, *56*, 227−241.
(31) Kuroki, S.; Ando, S.; Ando, I.; Shoji, A.; Ozaki, T.; Webb, G. A. Hydrogen-Bonding Effect on 15n Nmr Chemical Shifts of the Glycine Residue of Oligopeptides in the Solid State as Studied by High-Resolution Solid-State Nmr Spectroscopy. *J. Mol. Struct.* **1990**, *240*, 19−29.
(32) Schultz, E.; Nissinen, E. Inhibition of Rat Liver and Duodenum Soluble Catechol-O-Methyltransferase by a Tight-Binding Inhibitor or-462. *Biochem. Pharmacol.* **1989**, *38*, 3953−3956.
(33) Rod, T. H.; Ryde, U. Accurate Qm/Mm Free Energy Calculations of Enzyme Reactions: Methylation by Catechol O-Methyltransferase. *J. Chem. Theory Comput.* **2005**, *1*, 1240−51.
(34) Kulik, H. J.; Zhang, J.; Klinman, J. P.; Martínez, T. J. How Large Should the Qm Region Be in QM/MM Calculations? The Case of Catechol O-Methyltransferase. *J. Phys. Chem. B* **2016**, *120*, 11381−11394.
(35) Wang, S.; Hu, P.; Zhang, Y. Ab Initio Quantum Mechanical/Molecular Mechanical Molecular Dynamics Simulation of Enzyme Catalysis: The Case of Histone Lysine Methyltransferase SET7/9. *J. Phys. Chem. B* **2007**, *111*, 3758−3764.

DOI: 10.1021/acscatal.9b00174
ACS Catal. 2019, 9, 4394−4401